



## Research papers

## Wave growth and forecasting in variable, semi-enclosed domains

M. Alomar<sup>a,\*</sup>, A. Sánchez-Arcilla<sup>a,1</sup>, R. Bolaños<sup>b,2</sup>, A. Sairouni<sup>c,3</sup><sup>a</sup> Maritime Engineering Laboratory/Universitat Politècnica de Catalunya (LIM/UPC), C/Jordi Girona 1-3, Edif.D1, 08034 Barcelona, Spain<sup>b</sup> DHI, Agern Allé 5, DK-2970 Hørsholm, Denmark<sup>c</sup> Catalan Meteorological Service (SMC), C/Berlín 38-48 4a, 08029 Barcelona, Spain

## ARTICLE INFO

## Article history:

Received 16 May 2013

Received in revised form

4 May 2014

Accepted 8 May 2014

Available online 28 May 2014

## Keywords:

Fetch-limited

Sharp-gradients

Wave growth

Wave modelling

SWAN

Mediterranean Sea

## ABSTRACT

The accuracy of wave models in semi-enclosed-basins and orography-controlled wind conditions, especially during fetch-limited storm events, is known to be limited. Wind wave forecasting in the NW Mediterranean Sea is particularly demanding due to the characteristic sharp gradients of the wind and wave conditions. In this work we focus on the commonly observed underestimation of wave parameters even when the wind field is “correct” or overestimated. This is a small step to analyse such a discrepancy, where wind overestimation has been commonly used to get the “right” wave predictions for the “wrong” reason. Here we selected a suitable combination of nested meteorological and wave models to focus on the physics (in parameterized terms) of meso-scale wave generation in restricted domains. First, to better capture the typical sharp gradients in wind and wave fields under those conditions, the spatial resolution of the atmospheric model was progressively increased during a characteristic storm event from 18 km to 4 km; the corresponding frequency of the wind input was increased from 6 to 1 h. Second, the calculated rate of wave growth in the numerical model (i.e. the balance between the input term and the whitecapping dissipation) was analysed and tuned to match the observed local rate of wave growth. The rate of non-dimensional growth in the region of study, which was calculated using measurements along the fetch, turned out to be faster than simulated with the initial model settings and faster than reported in previous studies. Adjusting the wave growth rate in the model to the observations improved the estimated wave height by about 18% and the wave period by about 4%. Decreasing the grid size of the numerical models from 12 km to 4 km improved the timing of the wave peaks but not the maximum values of the storm. Increasing the frequency of the wind input (from 6 to 3 h) improved the estimation of the maximum wave height values (peaks) of the storm by about 13%. Summarizing, the results of this work showed that using high resolution and physically adjusted parameterizations in complex regions with strong wind and wave gradients such as the study area, it is possible to significantly reduce the under-estimation of wave parameters and to locally improve wave growth forecasting.

© 2014 Elsevier Ltd. All rights reserved.

## 1. Introduction

Wind generated waves result from the transfer of wind momentum and energy from the atmosphere to the sea via their interface or free ocean surface. Although for open sea conditions the basic processes are relatively well-known (for practical wave prediction purposes at least), the corresponding wave generation and evolution in semi-enclosed domains remains a subject of research, with important discrepancies between simulations and observations.

The predictability of wave fields in the North Western Mediterranean, considered in this paper, illustrates the pitfalls of fetch limited and duration limited generation under sharp wind gradients in time and space typical of the area (Sánchez-Arcilla et al., 2008). The accuracy of the predictions under such conditions is known to be limited compared with the open sea (Cavaleri and Bertotti, 1997). More precisely, there exists a serious underestimation of wave height under storm peaks and a corresponding overestimation under relatively calmer conditions (Bolaños et al., 2007), which has sometimes been solved by increasing the forcing wind speed (Cavaleri and Bertotti, 1997). However, the wind speed is not always under-estimated, as we will see in the study case presented in this work, and exploring alternative, physically based means to address the common underestimation of wave parameters in coastal areas is increasingly needed.

Sánchez-Arcilla et al. (2008) point to wind variability as the main source of error in wave forecasting in the region because of

\* Corresponding author. Tel.: +43 676 82058864.

E-mail addresses: [marta.alomar@hotmail.com](mailto:marta.alomar@hotmail.com) (M. Alomar), [agustin.arcilla@upc.edu](mailto:agustin.arcilla@upc.edu) (A. Sánchez-Arcilla), [rbol@dhigroup.com](mailto:rbol@dhigroup.com) (R. Bolaños), [asairouni@meteocat.cat](mailto:asairouni@meteocat.cat) (A. Sairouni).<sup>1</sup> Tel.: +34 93 401 64 68.<sup>2</sup> Tel.: +45 4516 9580.<sup>3</sup> Tel.: +34 93 567 60 90.

the high sensitivity of wave models to wind field variations. So far, most of the work carried out to include the effect of wind variability in wave predictions focused on the smaller temporal scales and gustiness. For example, the sensitivity of wave models to increased gustiness (small scale variability) was explored numerically by authors such as [Abdalla and Cavaleri \(2002\)](#) and [Ponce de León and Ocampo-Torres \(1998\)](#), among others. The results from their work indicate that the higher variability induced by gustiness results in increased wave parameters (wave height and peak period).

In addition to the mechanisms mentioned above, [Babanin and van der Westhuysen \(2008\)](#) point to an increased drag coefficient in gusty wind conditions, which enhances the transfer of energy from wind to waves. This energy transfer from wind to waves is commonly parameterized using the rate of wave growth, which changes depending on the wind and wave conditions ([Kahma and Calkoen, 1992](#); hereafter KC92).

Inspired by these promising outcomes, in the present work we focused on improving wave estimations by including in the wave model the wind variability at scales larger than turbulence both in time (h) and space (km), i.e. the mesoscale. The present study is, thus, considered a necessary contribution to the state of the art since it addresses the problem of underestimating the wave parameters without unnecessarily increasing the wind forcing, applying the knowledge and simulation capabilities available for gusty scales to meso-scale processes. Within these settings, in this paper we explore the limits of wave prediction capabilities in semi-enclosed domains and during wave growth conditions. Better understanding and predicting wave growth is the starting point that should then allow, in future work, more complex and common situations such as bimodal events and mixed seas to be addressed. In particular, we focus on a characteristic fetch-limited storm event, with no detectable swell to avoid further complexity, and we improve the estimation of its wave parameters using two different, but complementary, approaches.

1. Increasing the spatial and temporal resolution of the wind and wave models using a sequence of nested simulations. The ability to capture strong gradients using increased resolution models was addressed by [Bertotti and Cavaleri \(2009\)](#) who decreased the wave model's grid size to  $7 \times 5 \text{ km}^2$  (the wind input frequency was 3 h). These authors confirmed that wind estimations improve when increasing the resolution of the wind models because smaller scale features are better estimated. The resolution increase carried out in the present work complemented the results from the previous authors because, although also using high spatial resolutions, the wind input frequency was increased even more (up to 1 h instead of 3 h) in order to capture the variability during local short-duration (less than 12 h) storm events. This approach also addresses the seldom considered issue of the transmission of information within the model grid, which is of particular interest for sharp spatial gradients.
2. Calculating the rate of wave growth from in-situ observations and adjusting the rate of wave growth in the numerical model accordingly. This approach is based on the balance of the wave energy input and the dissipation terms, both from physical and numerical origins. Note here that whitecapping dissipation is right now the focus of recent research which attempts to improve it in spectral wave models (e.g. [Ardhuin et al., 2010](#)). In spite of all previous efforts, a definitive expression for dissipation due to whitecapping has not yet been agreed on. Therefore, adjusting the amount of whitecapping for local applications still is a more acceptable alternative to calibrate wave models locally ([Babanin and van der Westhuysen, 2008](#)).

Note again that the main goal of this work was to analyse the small scale differences between the simulations and the observed

time series at coastal scales. The methods used to reduce the observed discrepancies were based on the underlying physics because of this accurate and in detail analysis of the time series, instead of relying only in its statistical analysis, as it is commonly done in the state of the art.

The paper is structured as follows. In [Section 2](#) it presents the area of study, the Western Mediterranean Sea, and the case study considered. [Sections 3 and 4](#) address the two approaches taken to improve wave estimations: increasing the resolution of the model and adjusting the rate of wave growth to the observations. In [Section 3](#), the consistent over-prediction in wind velocity associated with increasing the spatial resolution provided an improvement of wave bulk parameters that still showed certain under-estimation, particularly for short duration, storm situations. In [Section 4](#), adjusting the rate of wave growth in the model to the slightly faster rate of wave growth from the observations also proved to reduce the consistent under-estimation of wave parameters. Finally, in [Section 5](#) we discuss the limitations of increasing the resolution in meteo-oceanographic models and how the restrictions of the commonly employed physical parameterizations condition the performance of the wave models. The road ahead for future improvements, combining numerical and observational advances, is also briefly considered.

## 2. Case study

### 2.1. Study area and time period

The Southern Catalan coast is located in the NW Mediterranean Sea ([Fig. 1](#) – upper plot). The area is characterized by a complex coastal orography, with the Pyrenees as the main orographic feature running in an E–W direction and several abrupt mountain ranges parallel to the coast i.e. in a NE–SW direction. During regional northern winds, the orography favours wind channelling down the Ebro River and off the Ebro Delta. The same applies to smaller river valleys, which are associated with ‘breaches’ in the coastal mountain range. These characteristic northwest land-to-sea winds (Mestral in the local vernacular) are particularly intense and persistent, especially during the fall and winter seasons. Fetch-limited wave growth controls northwest waves, the most frequent in the wave climate.

To assess the relative importance of the local wind patterns for wave generation we have selected a particular and characteristic wave storm event that was recorded within the RIMA-Med field campaign ([Alomar, 2012](#)). The case study is a complicated storm event in terms of wave predictions since it mainly consists of a highly variable northwest offshore wind field, representing fetch-limited wave growth. Northwest events are very common in the region and especially difficult to predict because of their intense nature and abrupt occurrence. The event selected for this paper occurred between 7 Dec. and 13 Dec. 2007.

The highest wind speed  $U_{10}$  (nearly 18 m/s) and significant wave height  $H_s$  (3.5 m) were measured at the most offshore station. Slightly lower  $U_{10}$  were recorded closer to the coast at the onset of wave growth (not shown). Wind direction during the event was relatively constant around  $295^\circ$ . Wind and wave instruments registered two peaks on the 8 Dec. at 00 h and on the 10 Dec. at 10 h, and a third but lower peak on the 9 Dec. at midday (see [Figs. 2 and 3](#)). This third peak had a slight swell component and could not be considered as pure sea (i.e. in [Section 4](#)). Peak wave directions were mainly from the NW, with peak periods ( $T_p$ ) ranging from 4 s to 7 s, depending on the distance to the coast (see [Fig. 2](#)).

The wave measuring instruments available in the studied area and during the event of interest are depicted in [Fig. 1](#) – upper plot.

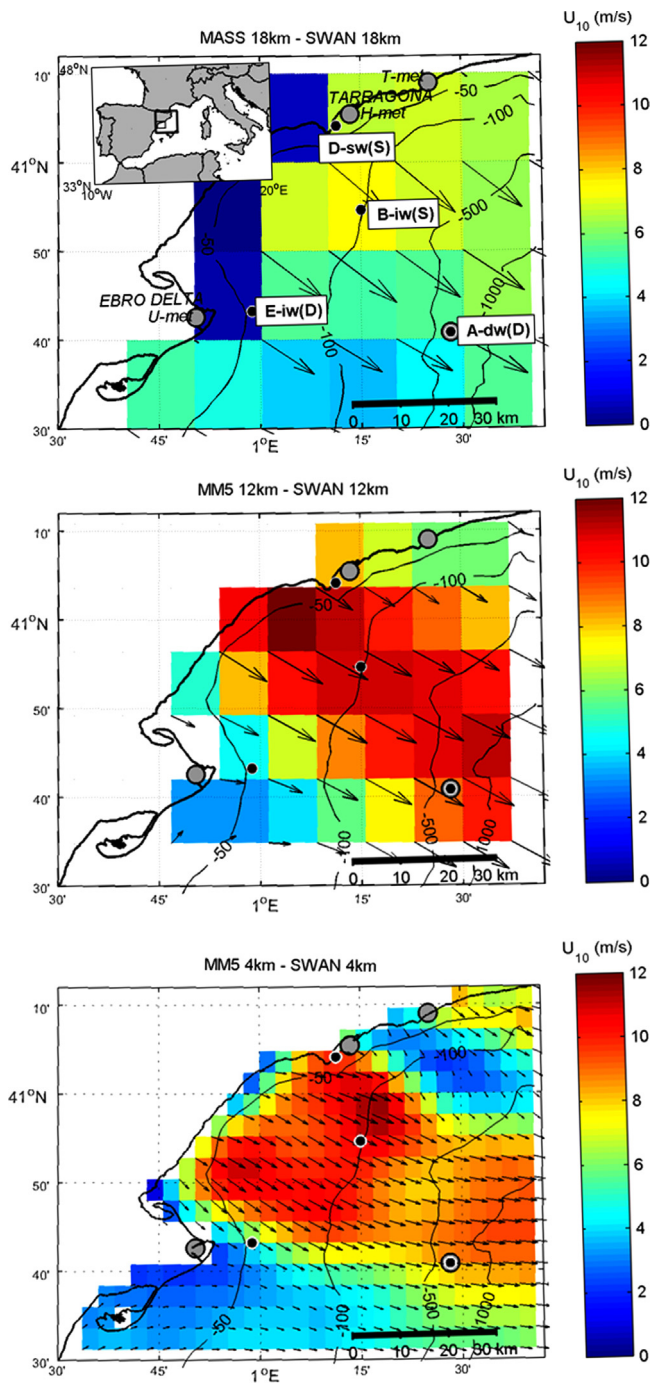


**Fig. 1.** Region of study and available instruments (upper panel) plus a comparison of the three atmospheric models and their spatial resolutions during a characteristic coastal wind jet: (top) MASS-18 km; (centre) MM5-12 km; (bottom) MM5-4 km. Colour and arrows show a snapshot of the wind velocity on the 7 Dec. 6h 2007. Wave recording instruments (black dots) and meteorological stations (grey dots) are depicted. Bathymetry is shown as black contour lines. In the top plot, the inner figure depicts the domain of WAM and SWAN-18 km (western Mediterranean). In the inner figure, the thick-lined square delimits the SWAN-4 km grid and the thin-line square within delimits the close-up of the study area depicted in the plots.

They were buoys located at different depths and distances from the coast: A-dw(D), B-iw(S) and E-iw(D). To make it easier for the reader to identify at a glance the characteristics of each buoy throughout the paper, the capital letter is a reference name for the instrument and is followed by a pair of lower case letters which indicate the depth of the instrument (*dw*, *iw*, *sw* – deep,

intermediate and shallow waters, respectively), and a bracketed letter indicating whether the available data are directional (D) or scalar (S). The set of buoys were approximately located along the mean direction of the NW offshore winds. The instrument farthest off-shore was A-dw(D). Buoys B-iw(S) and E-iw(D) had a similar fetch during off-shore wind events.

Wind speed and wind direction were recorded at four different meteorological stations: the deep water meteo-oceanographic buoy A-dw(D), a coastal-sea station located on Tarragona's harbour breakwater (H-met), and two coastal-land automatic meteorological stations T-met (north of the port), and U-met (south of the port). T-met data were provided by Tarragona's Port Authority. H-met and U-met were provided by the Catalan Meteorological Service (SMC). The location of each station is shown in Fig. 1 (top panel). We have also used near real time blended surface wind data obtained by blending ECMWF analysis data with remotely sensed data every 6 h at  $0.25^\circ$  spatial resolution. More details on the blending process can be found in Bentamy et al. (2007).

## 2.2. Meteo-oceanographic fields

The wind fields at different spatial resolutions and frequency used to simulate the storm event of interest have been obtained from two different models both run operationally at the SMC, following their calibration and accuracy protocols. The coarser resolution simulation were obtained from MASS (Mesoscale Atmospheric Simulation System) and the finer resolution simulations were obtained from MM5 (Fifth Generation Mesoscale Model). The MASS model is a mesoscale limited area model based on a primitive equation system and vertical sigma levels. A hydrostatic version (MASS 5.13) is currently running operationally at the SMC using as input and boundary conditions the GFS with  $0.5^\circ$  resolution data. Daily operational runs include two simulations (18 km and 8 km) every 12 h, all of them with 21 vertical sigma levels; output wind fields are provided every 6 h. More information on MASS wind fields as a forcing into spectral models can be found in Bolaños et al. (2007).

MM5 vs.3.5 is a nonhydrostatic primitive-equation model that uses terrain following sigma coordinates (Grell et al., 1994). It is running operationally for the Catalan coast at the SMC since 2008 with a spatial resolution of approximately 15 km. The higher resolution wind field simulations used in this work were obtained running MM5 at 36 km resolution and subsequently nesting at 12 and 4 km resolution. The 36 km resolution mother domain covered southwest Europe, the second domain covered Catalonia and south France and the finer domain covered only Catalonia and its coastal sea (northeast Spain). The initial and boundary conditions for the 36 km model correspond to the ECMWF predictions with  $0.5^\circ$  resolution data every 24 h. Surface observations (METAR, SAO, SHIP) and upper air sounding data (RAOB data) were assimilated into the 36 and 12 km resolution simulations, which were then used as initial conditions for subsequent nestings. The wind output frequency was 6, 3 and 1 h for the three different grids. For more information refer to Alomar (2012). The differences between the models are, basically, the different initial and boundary conditions: the Global Forecast System, GFS, in MASS and the European Centre for Medium-Range Weather Forecasts, ECMWF, and data assimilation in MM5. In this work the emphasis of the search for the best winds available has been placed on the spatial and temporal resolution and the accuracy compared to local observations, rather than on the differences between atmospheric models.

In this work we also used two slightly different spectral wave models for the purpose of comparing the parameterization of the physical terms in each model, as addressed in Section 4. The wave model running operationally for the Catalan coast is WAM Cycle 4

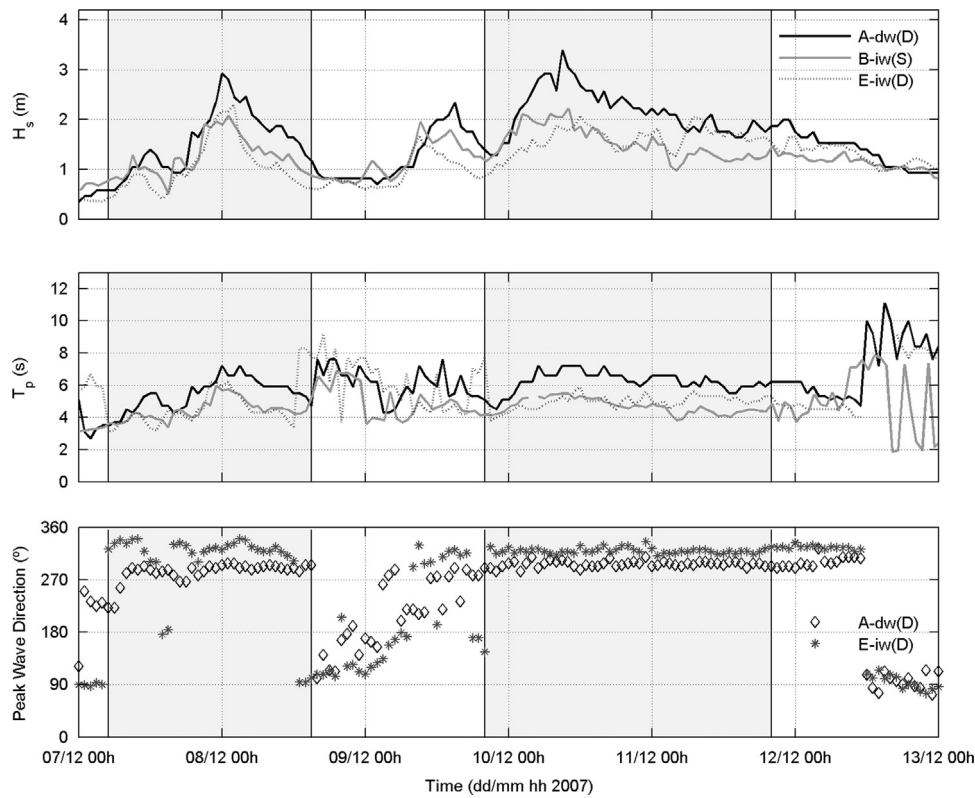


**Fig. 2.** Significant wave height (upper plot), peak period (middle plot), and peak wave direction (lower plot) from 7 December to 13 December 2007 (the studied storm event) at the different wave instruments. The grey background indicates the period used to calculate the rate of wave growth (7 December 5 h – 8 December 15 h and 9 December 20 h – 11 December 20 h).

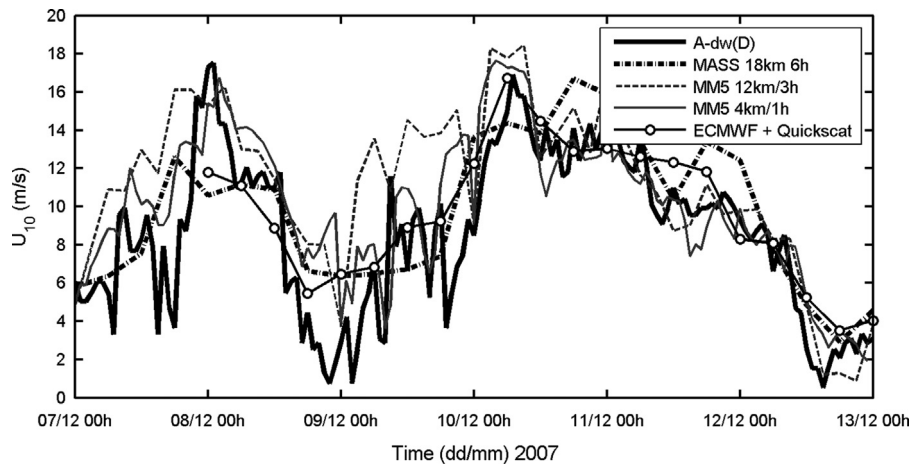


**Fig. 3.** Modelled wind speed time series from MASS 18 km/6 h, MM5 12 km/3 h, MM5 4 km/1 h, ECMWF+QuikSCAT data and observations at the location of the offshore buoy A-dw(D). The reproduced periods goes from 7 December to 13 December 2007.

(Monbaliu et al., 2000). The second spectral model we have used is SWAN (Simulating Waves Nearshore; version **SWAN 40.72ABCD**), which is specifically designed for coastal areas (Booij et al., 1999). Both models are based on the action balance equation for given source and sink functions. However, SWAN uses an implicit scheme for wave propagation, which is computationally more economic in shallow waters than other state-of-the-art third generation models (including WAM), and claims to provide additional robustness to the model. In WAM, wind input and dissipation formulations depend on the existing sea state and are taken from Janssen (1991), hereafter referred to as JAN. In SWAN deep water physics are taken by default from a previous version of the WAM model and are due to Komen et al. (1984), hereafter referred

to as KOM. In SWAN it is also possible to use JAN formulations, as well as the dissipation term introduced by Van der Westhuysen et al. (2007). In this work SWAN was run with the KOM parameterizations; the comparisons performed in Section 4 showed that for deep waters and equal domains and drivers, both models presented non-significant differences

### 3. High resolution simulations

In this section we explore the limits of wave modelling in semi-enclosed domains using improved wind fields and higher resolution wind and wave models. The resolution increase aimed to

**Table 1**  
Wind and wave model settings for the different numerical simulations performed in the studied storm event.

Run name	Wind input			Wave output	
	Wind model	Spatial resolution (km)	Input frequency (h)	Wave model	Spatial resolution (km)
WAM SWAN	MASS	18	6	WAM SWAN	18
MM5 12 km/6 h MM5 12 km/3 h	MM5	12	6 3	SWAN	12
MM5 4 km/3 h MM5 4 km/1 h	MM5	4	3 1	SWAN	1

avoid smoothing wind and wave peak values and to capture wind and wave spatial structures typical of sharp-gradient regions. The analysis was done by hindcasting the fetch-limited storm case with characteristic highly variable winds. We used (Table 1) wind fields at three spatial grid resolutions (18 km, 12 km, and 4 km) and three wind input frequencies (6 h, 3 h, and 1 h) to drive spectral wave models at four spatial resolutions (18 km, 12 km, 4 km, and 1 km).

### 3.1. Modelling strategy

To address the effects of increasing the spatial resolution of the input wind fields we compared wave estimations obtained from forcing the wave model with various high resolution winds. The set of simulations used is summarized in Table 1. The simulations were compared to assess the improvement of wave estimations due to an increase of the spatial resolution and the input frequency of the forcing wind fields.

Note that the same forcing wind fields (the operational MASS atmospheric model at SMC), were used in the first couple of simulations to compare the two different wave models (WAM and SWAN). This comparison mainly served to assess the different wind input and dissipation formulations implemented by default in each model. This comparison showed that both models missed the first  $H_s$  peak of the storm, in agreement with the under-prediction of the corresponding  $U_{10}$  peak in MASS. Nonetheless, the second and third  $H_s$  peaks were also importantly under-predicted and  $U_{10}$  could not be directly blamed for this. In this work, we chose SWAN over WAM to further discuss the models' limitations under variable wind conditions because 1) SWAN overall predicted slightly better the  $H_s$  series; 2) WAM wind growth formulations were also available in SWAN and could be compared easily; 3) SWAN used a semi-implicit scheme that was less restrictive than WAM with regard to time step and spatial resolution.

The SWAN wave model was run in the local domain depicted in Fig. 1 and was not nested in a bigger domain because the considered storm event had no or very little interfering swell. A comparison of a model simulation of this particular storm event with or without nesting in a larger domain (with swell) showed that the overall wave height differences were not relevant ( $< 0.02$  m at the peaks; not shown).

In the numerical experiment the bottom friction was not activated and neither were the triads or the depth-induced breaking because these processes are only important in shallow waters with 'enough' propagation length. We mainly considered growing waves from the coast towards offshore and, because in the region of study the water depth increases rapidly, deep water conditions could be assumed in the majority of the domain. The main physical

processes (source functions) active during this experiment were wind input, dissipation through whitecapping and quadruplet interactions. The non-linear interactions were resolved using the DIA approximation. The integration time step was set to 20 min, the numerical scheme was a first order scheme (BSBT) with the number of iterations set to 15. The frequency range was set to 0.04–1 Hz and the frequency resolution was distributed logarithmically ( $\Delta f/f=0.1$ ) in order to comply with the DIA approximation. The directional resolution was set to  $10^\circ$ .

The comparison between simulations was based on two main statistical variables: the slope of the best-fit line through the origin minus 1 (slope – 1) of the scatter plot (simulated versus observed data) and the  $R^2$  coefficient that described the amount of variability captured by the simulation. Note that because the data compared are bounded and always positive ( $U_{10}$ ,  $H_s$ , and  $T_p$ ) we have log-transformed them. The parameter slope is the exponential of the independent variable ( $x$ ) in a regression equation where the slope is forced to be 1 and the variables have been log-transformed. A direct result of the log-transformation is that the parameter slope-1 can be conveniently used as a measure of the proportion of over/under-estimation (bias) of the simulation (dependent variable  $y$ ) versus the observed data (independent variable):

$$y = x^{\text{slope}}$$

The coefficient of determination  $R^2$  used to measure the efficiency of the fit is 1 minus the quotient of the variance of the residuals (i.e. the distance from the forecast model  $f_i$  to the fit  $y$ ) over the variance of the forecast model:

$$R^2 = 1 - \frac{\text{Var} [\text{residuals}]}{\text{Var} [\text{total}]} = 1 - \frac{\sum_i (y_i - f_i)^2}{\sum_i (y_i - \bar{y})^2}$$

$R^2$  measures the percentage of variability of the forecast model consistent with the buoy data, and is usually expected to be independent of the scale of the phenomena compared. Therefore, the larger  $R^2$  value the more natural variability is captured by the forecast model. Note that, compared with the standard coefficient of determination,  $R^2$  can be negative indicating that the obtained fit explains the variability of the forecast model worse than no fit at all (or the mean of the model data  $\bar{y}$ ); refer to Alomar (2012) for more details.

### 3.2. Wind field accuracy

The main goal of this article was to explore the performance limits of wave models in coastal domains, rather than carrying out a meteorological analysis of the wind forcing. For this reason, we had to make sure that the employed wind fields where the best available in the studied area with the desired time and space resolution. In this section we, thus, show the accuracy of the simulated wind fields that were later used to force the wave models.

The accuracy of the simulated wind fields used was assessed by comparing the time series of simulated wind speed (at the location of the four meteorological stations) with the observations, using statistical tools and visual analysis. The input wind fields compared in this work were those summarized in Table 1. In Fig. 3, the time series of measured  $U_{10}$  are compared with the simulated  $U_{10}$  time series from the different model simulations (at different resolutions) at the location of the deep water buoy A-dw(D). It is shown how the simulations with a higher temporal variability (1 and 3 h) are better than the simulations from the operational models (6 h). The highest values of  $U_{10}$  were significantly better reproduced by higher resolution simulations (MM5), both in

magnitude and timing. Also, the finer-resolution simulations reproduced local wind jets (peaks) that were not captured by the coarsest resolution simulations from MASS (see Figs. 1 and 3), and they accurately simulated the growth and decay rates of the wind speed peaks (see Fig. 3). Statistically, all simulations (both from MASS and MM5 at the different resolutions) over-estimated the observations (see Table 3). The highest  $U_{10}$  over-estimations were observed at the land stations (T-met and U-met).  $U_{10}$  best estimations were obtained at the coastal-sea station H-met and at the most offshore buoy A-dw(D).

The lowest wind speed over-estimation rates were given by the coarse temporal resolution MASS model. However, the  $R^2$  coefficient (which is independent of scale) indicated that higher resolution runs (MM5) simulated a larger per cent of the variability contained in the observed data, compared with the low resolution runs. Note here that the rugosity coefficient over the sea surface was set to 0.01 cm for MM5 and 0.03 cm for MASS as initial values. The results from the comparison of MM5 at 12 km spatial resolution and the nested MM5 at 4 km resolution indicated that increasing the spatial resolution reduced the over-estimation of  $U_{10}$  from 33% to 27% at the offshore buoy A-dw(D) (see Table 2). Note that Cavalieri and Bertotti (2003) suggested using higher resolution models to obtain higher  $U_{10}$  and to compensate the usually under-estimated  $U_{10}$  at the scales they were working with (approximately 190–30 km). In this work the increase of spatial resolution was done at even smaller scales (12 km to 4 km). This refinement reproduced better the local topography and it reduced  $U_{10}$  over-estimations at sea. The end result was the same as that reported in previous studies: wind speed estimations at sea were improved when increasing the model's resolution. The most accurate wind fields available for the case study corresponded to the highest-resolution simulation (4 km; 1 h).

The spatial accuracy of the wind fields was also assessed by comparing the time series from the real time blended surface wind data (ECMWF+Quikscat); see Fig. 3. Note again that although the variability of the wind time series is well captured by the high resolution models, a general over-estimation of the wind speed exists. For the purpose of this work, the reader should thus bear in mind that the simulated wind fields are not necessarily the main responsible factor for the commonly observed under-estimation of the wave parameters.

### 3.3. Wave fields accuracy

#### 3.3.1. The role of the spatial resolution

We have shown in the previous section that all simulated wind fields over-estimated the wind observations at the meteorological stations (Table 2 and Fig. 3). Nonetheless, the simulated  $H_s$  values were under-estimated at all locations (Table 3). Statistically, the best  $H_s$  values were obtained when using  $U_{10}$  from the 12 km resolution simulation, partially, because it provided the largest overestimations of  $U_{10}$ . In Fig. 4, it is shown that the three  $H_s$  peak values were better estimated when using MM5-12 km. Increasing the wind spatial resolution from 12 km to 4 km, although improving  $U_{10}$  estimations and the timing of the peaks, also enhanced the

underestimation of both  $H_s$  and  $T_p$ . A 33% over-estimation in  $U_{10}$  from MM5-12 km resulted in an 8% over-estimation of  $H_s$  at A-dw(D); and a 27% over-estimation of  $U_{10}$  from MM5-4 km resulted in a 10% under-estimation of  $H_s$  at the same buoy.  $T_p$  under-estimation was also enhanced with higher resolution wind fields, but it was less sensitive to the wind decrease than  $H_s$  (see Table 4).

The decrease in grid size of the wave model (1 km) did not significantly improve the estimations of the wave parameters unless the grid size of the wind field was also decreased (4 km). Instead,  $H_s$  decreased more due to the higher diffusivity of the numerical scheme (BSBT) for larger discretizations of the computational grid, as we will discuss in Section 5.

#### 3.3.2. The role of (wind input) time resolution

The careful analysis of the observed wind speed time series during the study period indicated that  $U_{10}$  could increase by a factor of 2 in one hour. The wind observations considered in this study were the mean of 10 min records every hour, while smaller variations of wind speed within the hour describe smaller scale processes (turbulence or gustiness). In this study, we increased the temporal resolution of the wind input from the operational 6 h to 1 h, thus focusing on the mesoscale patterns rather than in the smaller scale of wind gustiness, and we assessed the resulting changes on the simulated wave fields.

To assess the impact of increasing the wind input frequency in the wave model we first evaluated  $H_s$  and  $T_p$  from SWAN when forced with MM5-12 km and wind input every 3 h and we compared it with a wind input frequency of 6 h (using the wind field from +00 h to +18 h, every 6 h). The results in Tables 3 and 4 indicated that increasing the input frequency resulted in increased  $H_s$  and  $T_p$  at all locations. The differences were not important statistically, but they were especially relevant in the visual analysis during the peaks of the storm, where the maximum values were better estimated, as shown in Fig. 5. Increasing the input frequency in MM5-12 km from 6 to 3 h increased the wave height about 0.44 m (13%) during the third storm peak. Thus, with an increase in the wind input, the under-estimation of the maximum value (3.4 m) decreased from 17% (6 h) to 4% (3 h). At the intermediate-water buoys, the difference was not as large (approximately 0.2 m; not shown here). Again,  $T_p$  was seen to be less influenced by temporal resolution changes than  $H_s$ , as expected since most of the activity occurs at high frequencies.

An increase of the input frequency from 3 to 1 h was analysed in terms of the high resolution MM5-4 km wind fields; Fig. 5 shows that only minor improvements were achieved. The maximum values of the three main  $H_s$  peaks increased slightly, but the  $H_s$  under-estimation remained large (up to 0.5 m at the peak). An interesting behaviour of the wave model was observed during the last two days of the storm: the wind input every 3 h generated two sudden wave height peaks (11 and 12 Dec.) that disappeared when the wind input every 1 h was used (Fig. 5). The wave peaks were seen to be a consequence of two wind peaks simulated by MM5-4 km (see Fig. 3). These two simulated peaks were not observed either in the wind or in the wave measurements and were thus, considered spurious results of these numerical settings.

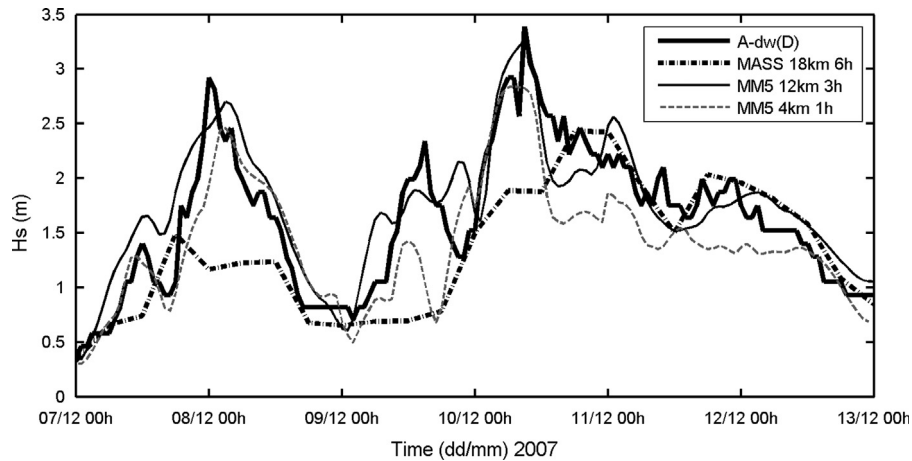
**Table 2**

Comparison of the logarithm of the modelled wind speed ( $U_{10}$ ) and the observations from 7 Dec. to 13 Dec. 2007. Boldfaced values (first column for each model configuration) correspond to the slope of the regression equation minus 1, termed "slope - 1", (positive/negative values indicate an over/under-prediction). Regular values (second column for each model configuration) correspond to the determination coefficient  $R^2$ .

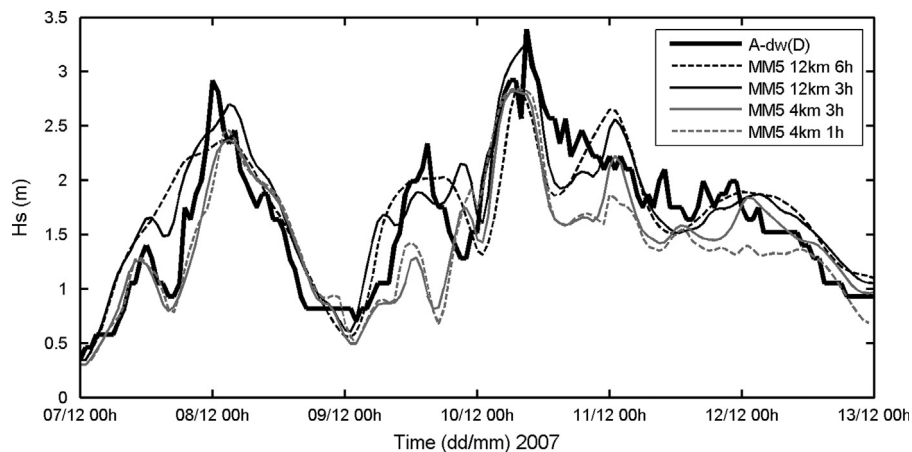
$U_{10}$	MASS 18 km-6 h		MM5 12 km-6 h		MM5 12 km-3 h		MM5 4 km-3 h		MM5 4 km-1 h	
A-dw(D)	<b>0.19</b>	0.37	<b>0.27</b>	0.55	<b>0.33</b>	0.44	<b>0.27</b>	-0.19	<b>0.28</b>	-0.08
H-met	<b>0.23</b>	-0.95	<b>0.16</b>	0.21	<b>0.09</b>	-0.01	<b>-0.04</b>	-0.18	<b>-0.14</b>	-0.34
T-met	<b>1.73</b>	-3.22	<b>1.14</b>	-0.72	<b>1.05</b>	-0.79	<b>1.08</b>	-0.81	<b>0.98</b>	-0.60
U-met	<b>2.78</b>	-2.21	<b>2.20</b>	-1.13	<b>2.41</b>	-1.85	<b>1.79</b>	-1.60	<b>1.40</b>	-1.17

**Table 3**Comparison of the logarithm of the simulated and observed wave height ( $H_s$ ) from 7 Dec. to 13 Dec. 2007. See Table 2.

$H_s$	WAM	SWAN		MM5 12 km/6 h		MM5 12 km/3 h		MM5 4 km/3 h		MM5 4 km/1 h		
A-dw(D)	<b>-0.18</b>	0.5	<b>-0.15</b>	0.42	<b>0.07</b>	0.70	<b>0.09</b>	0.77	<b>-0.11</b>	0.73	<b>-0.13</b>	0.74
B-iw(S)	<b>-0.31</b>	0.41	<b>-0.23</b>	0.37	<b>0.01</b>	0.56	<b>-0.03</b>	0.57	<b>-0.15</b>	0.56	<b>-0.18</b>	0.56
E-iw(D)	<b>-0.29</b>	0.54	<b>-0.28</b>	0.52	<b>-0.08</b>	0.63	<b>-0.04</b>	0.56	<b>-0.25</b>	0.57	<b>-0.23</b>	0.62

**Fig. 4.** Wave height from 7 to 13 December 2007 estimated using wind inputs from three different sources: MASS-18 km, MM5-12 km and MM5-4 km. SWAN was run at 1 km spatial resolution using the BSBT numerical scheme.**Table 4**Comparison of the logarithm of the simulated and the observed peak period ( $T_p$ ) from 7 Dec. to 13 Dec. 2007. See Table 2.

$T_p$	WAM	SWAN		MM5 12 km/6 h		MM5 12 km/3 h		MM5 4 km/3 h		MM5 4 km/1 h		
A-dw(D)	<b>-0.12</b>	0.28	<b>-0.22</b>	0.33	<b>-0.12</b>	0.14	<b>-0.12</b>	0.36	<b>-0.21</b>	0.37	<b>-0.21</b>	0.48
B-iw(S)	<b>0.07</b>	-0.13	<b>-0.06</b>	-0.04	<b>0.00</b>	-0.9	<b>-0.01</b>	-1.00	<b>-0.11</b>	-0.71	<b>-0.1</b>	-0.32
E-iw(D)	<b>-0.07</b>	0.32	<b>-0.18</b>	-0.08	<b>-0.16</b>	-0.9	<b>-0.15</b>	-0.77	<b>-0.30</b>	-0.34	<b>-0.27</b>	-0.40

**Fig. 5.** Wave height from 7 to 13 December 2007 estimated using MM5 at different spatial resolutions (12 km, 4 km) and different temporal resolutions (6 h, 3 h, 1 h). SWAN was run at 1 km spatial resolution using the BSBT numerical scheme.

The different response of the wave model to the wind input every 3 h compared with 1 h indicated that the wave model needed a certain amount of time (3 h) to adjust and respond to the wind field. When the wind input was every hour, the wave model did not have enough time to respond to the wind signal (peak) and a corresponding wave peak was not simulated. This behaviour was also reported previously by others authors such as Niclasen (2006). This result indicated that changes in simulated  $H_s$  were slower than changes in the wind input. In this specific case, a slow response of the wave model compensated the errors in the wind

speed and the unrealistic peaks of MM5 4 km/1 h were not converted to unrealistic wave height peaks.

Wave height under-estimations were also observed at the shorter-fetch buoys B-iw(S) and E-iw(D). These results indicated that the wave response in the spatial domain (i.e. short fetches) was too slow compared with the observations. Niclasen (2006) already pointed out the need to improve the slow response of wave models in short fetches. He reached this conclusion after comparing wave growth curves from observations and SWAN (using JAN formulation) and observing that observations grew

faster than simulated in SWAN. If the wind input changes very fast (as it certainly does in the situations considered) the simulated wave field might not have enough time to respond and grow accordingly. Provided that wind to wave transfer under gusty wind conditions was seen to be enhanced (Abdalla and Cavaleri, 2002) it seemed logical to explore alternative parameterizations of wind variability in time (e.g. gustiness and mesoscales) to enhance wave growth in the region of study. In the next section we calculate the local rate of wave growth and we adjust the wave model accordingly.

#### 4. Wave growth

The presented numerical simulations and also observational evidence suggest that wave growth is enhanced in situations that deviate from the mostly homogenous wind conditions for which the default settings of wave models are tuned. Note here that the possible influence of the forcing terms in the wave model (e.g. KOM versus JAN) was dismissed when comparing the two wave models (WAM and SWAN) using the same grid size (18 km) and wind input frequency (6 h), as shown in the first two columns of Tables 3 and 4, for  $H_s$  and  $T_p$  respectively. Both wave models under-estimated the wave height at all locations, although SWAN's estimations were slightly better than WAM's. The best estimations were provided by both models at the most offshore buoy A-dw(D), with the longest fetch and more mature waves. These results showed that the differences between JAN (in WAM) and KOM (in SWAN) physical parameterizations were quantitatively not significant. Note also that the numerical implementation of the two models, although not identical, was not seen to make a significant difference either.

The calculated under-estimation in the wave parameters (during the case study) could not be corrected when using the default values in the model's parameterizations of wave growth (JAN and KOM). For this reason, we have calculated below the local non-dimensional wave growth curves (commonly used to tune wave models) using site specific observations. The resulting wave growth rate proved to be slightly faster than the reference values used to tune wave models. For this reason, and to assess the possibility to improve wave estimations in this way, we have adjusted the growth rate of the numerical simulations to the observations, and we assessed the improvement in wave estimations.

##### 4.1. Growth rate estimations

The use of non-dimensional growth curves to study wave growth along the fetch are thoroughly reviewed in KC92. The corresponding scaling laws are commonly used nowadays and represent non-dimensional energy and frequency (dependent variables) along non-dimensional fetch (independent variable). Within the spectral wave modelling community, the non-dimensional wave growth functions, and more specifically the parameterizations provided by KC92, are a reference method to calculate and quantify wave growth.

The scaling laws use the acceleration of gravity  $g$  and the wind speed  $U_{10}$  to non-dimensionalize the main wave parameters (wave energy  $E$  and peak frequency  $f_p$ ) and the fetch  $X$ . Non-dimensional wave energy ( $\bar{E} = g^2 E / U_{10}^4$ ) and peak frequency ( $\bar{f} = U_{10} f_p / g$ ) as a function of non-dimensional fetch ( $\bar{X} = gX / U_{10}^2$ ) are usually plotted on logarithmic axes. Then, the slopes of the regression lines correspond to the so-called development rate  $b$  of the dimensionless energy (and the downshift rate  $c$  of the frequency) along the dimensionless fetch. On linear axes the development rates can be written as  $\bar{E} = a_1 \bar{X}^b$  and  $\bar{f} = a_2 \bar{X}^c$ .

KC92 is the most widely used contribution on wave growth rates because it groups some of the most relevant fetch-limited experiments up to that time, including Hasselmann et al. (1973) (JONSWAP) and Donelan et al. (1985) (hereafter DO85). To that date, the development rates obtained from each experiment differed significantly because the stability of the atmosphere had not been taken into account. The development rates calculated in KC92 are close to, but lower than, 1 (see Table 5).

The wave data we employed to calculate the rate of wave growth is part of the specific offshore wind event described in Section 2. The data set did not comprise the whole storm period because some records containing residual swell were excluded. Such interfering swell was identified through an automatic spectral partitioning algorithm and a detailed visual analysis of the directional spectra from buoys A-dw(D) and E-iw(D) (see Alomar, 2012 for more details). Consequently, only wind sea data from North-western directions were considered; i.e. it was limited to the periods 7 Dec. 5 h – 8 Dec. 15 h and 9 Dec. 20 h – 11 Dec. 20 h (depicted by the darker regions in Fig. 2). This dataset was especially valuable because wind and wave conditions were relatively close to the ideal conditions encountered in the reference experiments; i.e. buoy measurements at different distances from the coast, wind direction perpendicular to the coast and no significant swell. Moreover, we used wind directions along the shore normal ( $315^\circ \pm 15^\circ$ ) only. The growth curves derived from the observations are plotted in Fig. 6 (left side) and are summarized in Table 6.

Additionally, we used the wave data from the numerical simulation of the storm called 'MM5 4 km/1 h' (in agreement with the nomenclature in the previous section; see Table 1) to calculate the wave development rate in the wave model and to compare it with the observations. Note that the development rates from the simulations presented in this work are not necessarily representative of the development rate of the SWAN model for all types of growth conditions, but they only correspond to the specific numerical simulation considered. The growth curves derived from the simulated wind and wave data are plotted in Fig. 6 (right side) and are summarized in Table 6.

The development rate  $b$  (exponent of the independent variable) calculated from local observations was slightly faster than the rate reported by KC92 and faster than the rate obtained from simulated data. The calculated downshift rate was very similar to the rate reported by KC92 in unstable atmospheric conditions and slightly slower than for the simulation. Note that the atmospheric conditions during most of the period of the study were unstable (i.e. the air temperature was lower than the sea temperature). KC92 reported

**Table 5**

Non-dimensional energy growth and frequency downshift functions calculated in earlier field experiments as reviewed in KC92 and Badulin et al. (2007).

Authors	Development rate ( $b$ )	Origin ( $a_1$ )	Downshift rate ( $-10\%c$ )	Origin ( $a_2$ )	Characteristics
Kahma and Calkoen (1992) – KC92st/KC92un	0.77	$9.3 \times 10^{-7}$	2.4	1.9	Stable atmosphere
	0.94	$5.4 \times 10^{-7}$	2.8	2.3	Unstable atmosphere
Donelan et al. (1985) – DO85	1	$2.8 \times 10^{-7}$	2.3	1.9	Stable atmosphere
	1	$3.8 \times 10^{-7}$			Unstable atmosphere

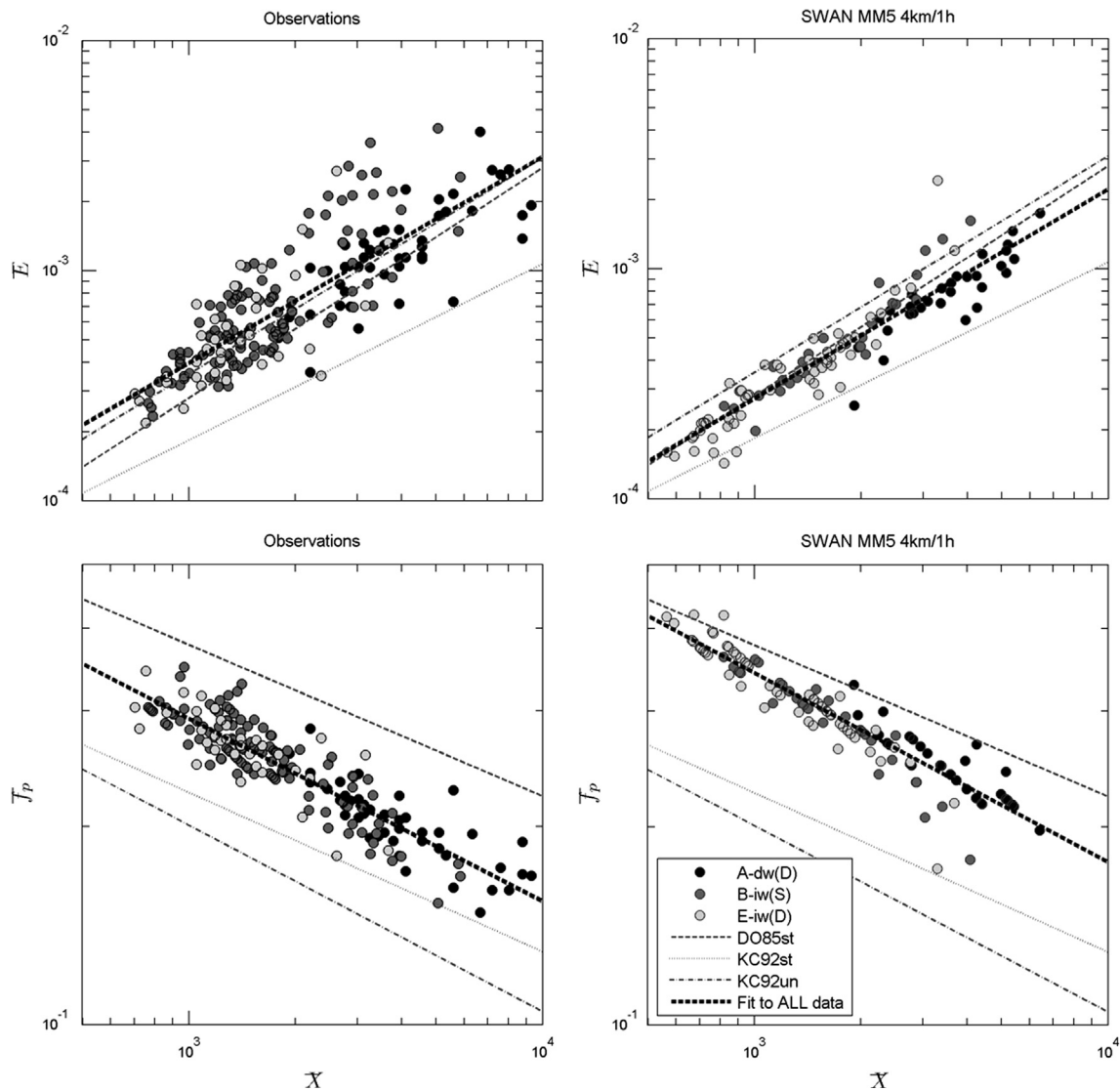


**Fig. 6.** Non-dimensional wave growth curves from observations (left) and from numerical simulations (right). Simulated data was obtained using MM5 4 km/1 h. Top panels show the energy growth curves and lower panels show the peak frequency evolution curves.

**Table 6**

Non-dimensional energy growth functions calculated from observations, MM5 4 km/1 h numerical simulation, and the reference values given in Kahma and Calkoen (1992) (KC92).

	Observations	Simulations	Reference KC92 Unstable conditions
Development rate $b$	$0.94 \pm 0.08$	$0.92 \pm 0.06$	0.92
Downshift rate $c$ ( $\times 10^{-1}$ )	$-2.81 \pm 0.18$	$-2.9 \pm 0.15$	-2.8

faster rates of wave growth during unstable atmospheric conditions. Although the atmospheric stability is not usually taken into account in wave models, this limitation is expected to be circumvented shortly, given the increasing availability of air and water temperatures in coastal domains.

Although the differences between simulated and observed data were not statistically significant, the graphical representation in Fig. 6 shows that the simulated energy was close to or below the theoretical curves. Observational data, instead, were generally above the curves. Bear in mind that low non-dimensional values mean that simulated energy (peak frequency) is lower (higher)

than the observations. The results above agree with the common wave under-estimations shown in the previous section even though the simulated wind speeds were closely (or slightly over-) predicted. Note also that the values in Table 6 are followed by the  $\pm 95\%$  confidence interval, which indicates that there is a 95% probability that the fit takes any of the values within that range. The confidence interval is also a measure of the scatter of the data points, with large intervals occurring when the scatter is large.

#### 4.2. Wave model tuning

The above results indicate that wave growth in this region, for these conditions, was slightly faster than considered by other authors and faster than simulated by the wave model. Consequently, tuning the regional wave model and adjusting the simulated wave growth rate to the slightly faster rate of wave growth should locally increase (decrease) the simulated energy (peak frequency) and should improve wave estimations. The performed calibration presented did not attempt to tune the model exactly to the growth curves. Our aim was to show that the improvement in the considered wave conditions was indeed possible when a faster wave growth was considered.

Calibrating spectral wave models (their source terms) using the non-dimensional wave growth curves have been commonly (and recently) used in the literature. Take for example the calibration of the new dissipation formulations derived by [Ardhuin et al. \(2010\)](#) and [Van der Westhuysen et al. \(2007\)](#). These authors used the growth rates derived by other authors (e.g. KC92) to calibrate wave growth for the general case; i.e. quasi-homogeneous wind conditions.

In this work we decided to tune the dissipation term in wave models to adjust the simulated growth rates to the observed ones. The main reason is that of all parameterizations involved in the balance of wave energy in spectral wave models (wind input, dissipation and non-linear interactions), the dissipation due to whitecapping is the worst know term “physically”. For this reason, the dissipation term is used to adjust the energy balance as a calibration term. Moreover, although a lot of work has been done towards improving the understanding and the parameterization of the dissipation source term (e.g. [Ardhuin et al. \(2010\)](#)), the precise physics of the dissipation due to whitecapping remains under discussion.

In this work, we have started from the dissipation source term suggested by KOM. To adjust this term to the observations, we focused on the fit coefficients in the expression for whitecapping, which is mainly controlled by the steepness of the waves. The steepness dependent coefficient  $\Gamma$  in KOM's expression for whitecapping was based on [Janssen \(1991\)](#) (according to [The SWAN Team 2009](#)), and is dependent on several coefficients. These coefficients depend on the expression of the wind input because they were obtained by closing the energy balance equation in idealized wave growth conditions (growing and fully developed waves) for deep waters. Note that for different wave growth conditions the tuneable coefficients could differ from the default values.

$\Gamma$  can be expressed as  $\Gamma = C_{ds}s^4stpm^{-2}$ . The dissipation coefficient  $C_{ds}$  is a linear coefficient of the amount of energy to be dissipated;  $C_{ds}$  in SWAN is by default  $2.5 \times 10^{-5}$ . The steepness parameter  $stpm$  ( $=\tilde{s}_{PM}^2$ ) should be considered the maximum steepness above which waves would break and dissipate energy through whitecapping. Small values of  $stpm$  consider that waves start breaking earlier in time, i.e. when they are less steep than for larger steepness limits;  $stpm$  in SWAN is by default  $3.02 \times 10^{-3}$ . Larger  $C_{ds}$  values and smaller  $stpm$  values result in larger dissipation. In SWAN 40.72ABCD it is possible to easily tune both  $C_{ds}$  and  $stpm$ .

Because the simulated growth rates were lower than the observed ones, the goal was to reduce the amount of whitecapping in the simulations (and to increase the generally under-estimated wave values). Thus, aiming to decrease  $C_{ds}$  and to increase  $stpm$ , we checked a few combinations of the tuneable coefficients and we adjusted the dissipation parameters of the KOM whitecapping formulation in SWAN.

The results in [Table 7](#) and [Fig. 7](#) indicated that tuning the dissipation term to adjust the model's growth rate to the observations slightly increased the estimated rate of wave growth and provided a generally better prediction of the wave time series.

In [Fig. 7](#) we observed, visually that the maximum values of the storm event were better estimated when decreasing  $C_{ds}$  to  $2 \times 10^{-5}$  and increasing  $stpm$  to  $3.5 \times 10^{-3}$ , compared with the default values in the SWAN wave model and compared with the other combinations of the coefficients.

The statistical results in [Tables 8](#) and [9](#) confirm the improvement achieved with the calibration of the wave model according to the observed wave growth rates. In agreement with the visual comparison, the improvements were especially relevant when decreasing  $C_{ds}$  to  $2 \times 10^{-5}$  and increasing  $stpm$  to  $3.5 \times 10^{-3}$ ; i.e. providing an improved fit (lowest slope-1 values or deviations from the fit) and comparably high  $R^2$  values (amount of variability captured in the simulation). Compared with the default values, in the best simulated case the wave height increased by about 18% and the peak period by about 4%. However, the under-estimation of the maximum values in [Fig. 7](#) indicated that numerical estimations still need to be improved in terms of both  $H_s$  and  $T_p$  (particularly for the consistent under-estimation of the peak period).

## 5. Discussion

Improved wave estimations were obtained in the study area by first, increasing the model's resolution (grid size and wind input frequency) and, second, adjusting the simulated wave growth rate to the observations. It was shown that improving wave estimations was indeed possible and both approaches contributed to noticeable progress. In other words, including mesoscale gradients (variability) into wave growth simulations, resulted in the most efficient approach to locally improve wave estimations. However, wave height and wave period remained under-estimated thus indicating that there still is room for improving wave modelling.

The input wind fields (the first main source of error; see e.g. [The WISE Group et al. \(2007\)](#)) were considered to have a relatively good accuracy; which was proved in [Section 3.2](#) from comparisons with measurements from both coastal and at-sea meteorological stations. The good accuracy was achieved both by using initial conditions from re-analysis and by decreasing the grid size (nesting) and increasing the wind output frequency, which permitted the better capture of the peaks of short-duration storm events and the local gradients in space and in time. In spite of the good point-wise accuracy achieved in the simulated wind fields, their lack of precision in representing the true wind patterns was apparent given the overall over-estimation of the time series.

In spite of the over-estimated input wind fields, wave parameters remained mostly underestimated; i.e. the accuracy of the wave estimations was poorer than that of the input wind fields. These results illustrate the tough challenge of meteo/wave models under limited and sharp gradient conditions, when compared with more homogeneous situations, such as those encountered in open oceans. Although in open oceans the main limitation is the wind fields, in semi-enclosed domains the low performance of the wave model suggests the need to reconsider the wave model itself.

According to [The WISE Group et al. \(2007\)](#), the second source of error in wave predictions is associated with the numerical settings selected to resolve numerically the action balance equation. Numerical limitations are especially relevant in association with the increase of the wind input resolution. The main numerical constraints of wave models are linked to the high diffusivity of low order numerical schemes, which require a reduced integration time step for decreasing grid sizes, and the stability of high order schemes, which need to fulfil the Courant number condition (thus imposing a necessary reduction of the grid size and the time step simultaneously). The reader is referred to [The WISE Group et al. \(2007\)](#) for a complementary discussion on the subject.

**Table 7**

Energy growth rates and 95% confidence interval obtained for different values of the dissipation coefficient  $C_{ds}$  (rows) and the maximum steepness  $stpm$  (columns).

$C_{ds} [\times 10^{-5}]$	$stpm [\times 10^{-3}]$	
	3 (default)	3.5
2	$0.93 \pm 0.06$	$0.95 \pm 0.06$
2.5 (default)	$0.92 \pm 0.06$	$0.94 \pm 0.06$

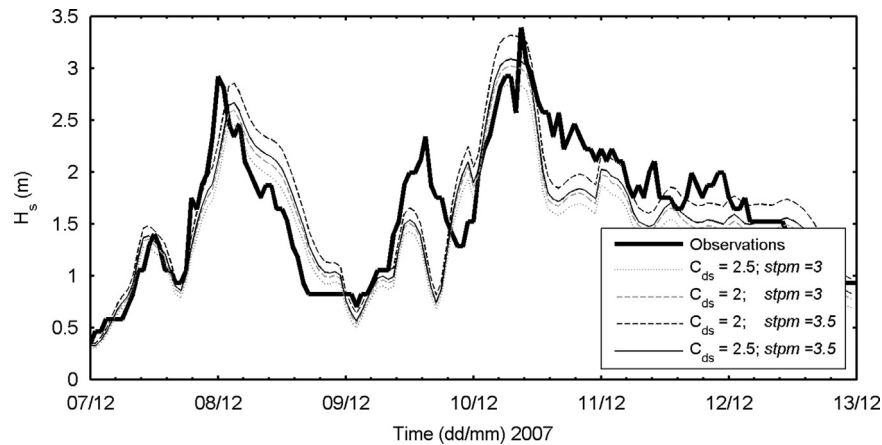


Fig. 7. Observed and simulated wave height at offshore buoy A-dw(D) during the fetch-limited wave storm that occurred from 7 to 13 December 2007 using different dissipation coefficients and maximum steepness.

**Table 8**  
Comparison of the logarithm of the simulated and the observed wave heights ( $H_s$ ) from 7 Dec. to 13 Dec. 2007. Boldfaced values correspond to the slope of the regression equation minus 1 slope – 1 (positive/negative values indicate an over/under-prediction). Regular values correspond to the determination coefficient  $R^2$ .

$stpm [ \times 10^{-3} ]$	3				3.5					
	2.5		2		2		2.5		3	
$C_{ds} [ \times 10^{-5} ]$										
A-dw(D)	<b>-0.13</b>	0.74	<b>-0.07</b>	0.42	<b>0.05</b>	0.72	<b>-0.04</b>	0.73	<b>-0.10</b>	0.74
B-iw(S)	<b>-0.18</b>	0.56	<b>-0.13</b>	0.56	<b>-0.01</b>	0.55	<b>-0.1</b>	0.55	<b>-0.16</b>	0.56
E-iw(D)	<b>-0.23</b>	0.62	<b>-0.18</b>	0.61	<b>-0.06</b>	0.61	<b>-0.14</b>	0.61	<b>-0.21</b>	0.62

**Table 9**  
Comparison of the logarithm of the simulated and the observed peak period ( $T_p$ ) from 7 Dec. to 13 Dec. 2007. See Table 8.

$stpm [ \times 10^{-3} ]$	3				3.5					
	2.5		2		2		2.5		3	
$C_{ds} [ \times 10^{-5} ]$										
A-dw(D)	<b>-0.21</b>	0.48	<b>-0.20</b>	0.47	<b>-0.17</b>	0.35	<b>-0.18</b>	0.40	<b>-0.21</b>	0.49
B-iw(S)	<b>-0.10</b>	-0.32	<b>-0.09</b>	-0.39	<b>-0.05</b>	-0.35	<b>-0.08</b>	-0.37	<b>-0.10</b>	-0.32
E-iw(D)	<b>-0.27</b>	-0.40	<b>-0.26</b>	-0.45	<b>-0.23</b>	-0.41	<b>-0.24</b>	-0.48	<b>-0.27</b>	-0.40

Numerical diffusion is particularly relevant for high-resolution simulations in semi-enclosed domains, where a resolution increase of the input wind fields needs to entail a matching decrease of the wave model's grid size in order to capture the sharp gradients. But small grid sizes require a decrease of the integration time step (to avoid numerical diffusion) with the corresponding increase of the model's computational time. During our case study, the under-estimation of the maximum values of the storm could be reduced and the timing of the storm peak could be slightly improved by reducing the integration time step of the wave model from 20 min to 10 min. However, the computational cost would double and the wave parameters would remain under-estimated (see Alomar 2012).

The third source of error mentioned in The WISE Group et al. (2007) is the parameterization of the physical processes in wave models. The wind input, energy dissipation, and non-linear interactions processes play a key role in semi-enclosed domains with short period waves so common near the coast of the NW Mediterranean. The three terms are balanced and should be considered together (see e.g. Rogers et al., 2003).

The parameterization of the balance of wind input and energy dissipation terms entrains a larger degree of uncertainty compared with the non-linear interactions. This uncertainty is derived from the limited knowledge of the exact processes describing the

transfer of energy between wind and waves, in particular within the dissipation term, whose spectral form in spectral wave models differs remarkably for each wind input parameterization. The reason is that the whitening term depends on a parameter that is estimated by closing the energy balance equation (source terms included) in fully developed conditions (see The SWAN Team, 2009). Additionally, the numerical scheme used to solve the source terms is constrained by the need of an unphysical term: the action density limiter (see e.g. Tolman, 2002). In this work we have only addressed the time series of the main wave parameters because this is the first and necessary step before addressing and discussing the effects on the wave spectra themselves. The rich information provided by spectral density functions was initially analysed in Alomar, 2012 but remains a pending topic for further improvement of wave modelling in restricted domains, where the wave nonlinearities and interactions should play a comparatively (with respect to deep water) more important role. Such a full spectral validation should allow an improvement of wave predictions under sharp gradients, particularly when satellite and radar observations will provide reliable wind and wave observations near the coast.

Of course, tuning the whitening term is not the only way to tune the balance of energy in wave models; the exact description of the energy input term is also uncertain and, to date, only

parameterizations are available (see e.g. KOM Komen et al. (1984), JAN Janssen (1991), Van der Westhuysen et al. (2007)). The uncertainties in the wave input term make clear that to estimate wave growth in rapidly changing situations a better understanding of the physical mechanisms of wind wave growth is needed. Calculating the rate of wave growth in the region of study was a small step in this direction. Note also that although the uncertainty with the non-linear interaction term is relatively small, in this work the DIA approximation was used; which applicability to multi-peaked or directionally-spread spectra (expected under sharp-gradient wind conditions) is questioned (The WISE Group et al., 2007).

The results of this work show the value of local adjustments to the growth curves. However, the universal validity and applicability of the non-dimensional wave growth curves had been already questioned (Badulin et al., 2007). In this direction, the capability of the non-dimensional curves as a method to estimate wave growth is limited mainly due to the large scatter of the measurements, to the deviations from ideal wind conditions, and to the limited suitability of using wind speed as the scaling variable in such variable conditions. Particularly demanding situations within wave growth parameterizations are the duration-limited stages of wave growth and the coexistence with more mature sea systems (see Alomar (2012) for more details).

The scaling laws used in this work to describe wave growth are the most widely used but not the only ones. For example, DO85 described wave growth as a function of the inverse wave age instead of the non-dimensional fetch. Also Badulin et al. (2007), among others, used alternative non-dimensional variables to calculate wave growth such as the wave dissipation rate. Nonetheless, we still lack a universally accepted method to describe wave growth particularly for variable conditions and small scales (from hour to days).

From a practical point of view, the results of this study can be implemented for the studied area and other semi-enclosed and variable regions, subject to further local validations in view of the underlying uncertainties. On the one hand, an increase in the spatial and temporal resolution would better capture the meso-scale phenomena in the region; i.e. the timescale of storms' onset and wind jets and the spatial scale of sharp-gradients that can be produced by particularities of the local topography. Nonetheless, increasing too much the spatial resolution can lead to an enhanced under-estimation of wave parameters due to numerical diffusivity or a much longer computational time. On the other hand, adjusting the rate of wave growth and implementing it in operational models requires, in general, an extensive calibration effort to effectively improve the wave predictions for the characteristic meteo-oceanographic patterns in the area.

## 6. Conclusions

Improving wave predictions in semi-enclosed domains such as the NW Mediterranean has proved a tough challenge for present wave models and will likely keep on offering a difficult physical problem for the coming years. The combination of fetch limited conditions, sharp gradients in time and space, and the simultaneous demand of robust and reliable wave forecasting for multiple coastal and offshore activities has been at the core of the present research.

The results obtained and presented in this paper indicate that a careful combination of the wave growth term and the nesting sequence may lead to a significant improvement of wave predictions in sharp-gradient regions. The short duration storm events typical of these domains require a high resolution in time and space that does not smooth out the highest wind speed peaks. The results showed

the advantages of increasing the resolution up to a point, beyond which any further refinement of resolution did not improve the results and did even deteriorate them if not accompanied by a corresponding improvement in the physical parameterizations.

In the region of study, the best wind speed estimations, compared with the observations, corresponded to a mesh size of 4 km and a time step of 1 h (reanalysis wind fields based on boundary conditions from ECMWF). Bear in mind, e.g. for operational applications, that the largest wave improvement corresponded to a frequency increase of the wind input from 6 to 3 h. This increased the wave height by more than 10% at the storm peak, thus reducing the common under-estimation of the wave parameters. Increasing the frequency of the wind forcing was more effective than the corresponding increase of the spatial resolution (from 12 to 4 km), which only improved the timing of the peaks but not the maximum values obtained. A further increase of the time frequency (up to 1 h) was largely ineffective, particularly when it was not accompanied by a corresponding increase of spatial resolution and an improved parameterization of the physical terms to counteract the slow response of the wave model. With minor adjustments of the numerical settings and using the proposed wave growth curves, the prediction of the significant wave height improved locally by about 20%.

The results presented also show the importance of re-examining the action balance for spectral wave models in semi-enclosed domains, where any modification of the wave growth terms should go hand in hand with the corresponding improvement of the energy dissipation term. The numerical dissipation should also be taken into account here, especially because it increases for such high resolution meshes. From the physical point of view, further research on the physics of wind and wave interactions, particularly for the early stages of generation and small scales (i.e. the mesoscale), is needed.

Following the results above and to characterize better the meso-scale processes and their interaction with a new family of coastal processes, extended data sets (in-situ and remote) are needed. Particularly in sharp-gradient regions, the required improvement in knowledge and models can only be based on intensive field campaigns.

## Acknowledgements

We would like to thank the reviewers and the editor for their patience and very helpful comments that made this document suitable for publication. The financial support for this research was provided by the following projects: RIMA (MEC, TRA2006-05132/TMAR), COVARIANCE (MEC, CTM2010-19709) and FIELD\_AC (FP7\_SPACE-2009-1 no. 242284). Also, we would like to thank the XIOM network, 'Puertos del Estado', and Tarragona Port Authority for sharing their valuable data.

## References

- Abdalla, S., Cavaleri, L., 2002. Effect of wind variability and variable air density on wave modeling. *J. Geophys. Res.* 107, 3080.
- Alomar, M., 2012. Improving Wave Forecasting in Variable Wind Conditions. The Effect of Resolution and Growth Rate for the Catalan Coast (Ph.D. thesis). (<http://www.tdx.cat/handle/10803/111230>).
- Ardhuin, F., Rogers, E., Babanin, A.V., Filipot, J., Magne, R., Roland, A., van der Westhuysen, A., Queffelec, P., Lefevre, J., Aouf, L., Collard, F., 2010. Semiempirical dissipation source functions for ocean waves. Part I: definition, calibration, and validation. *J. Phys. Oceanogr.* 40, 1917–1941.
- Babanin, A.V., van der Westhuysen, A., 2008. Physics of “saturation-based” dissipation functions proposed for wave forecast models. *J. Phys. Oceanogr.* 38, 1831–1841.
- Badulin, S.I., Babanin, A.V., Zakharov, V.E., Resio, D., 2007. Weakly turbulent laws of wind-wave growth. *J. Fluid Mech.* 591, 339–378.

- Bentamy, A., Ayina, H., Queffeuilou, P., Croize-Fillon, D., Kerbaol, V., 2007. Improved near real time surface wind resolution over the Mediterranean Sea. *Ocean Sci.* 3, 259–271.
- Bertotti, L., Cavaleri, L., 2009. Large and small scale wave forecast in the Mediterranean Sea. *Nat. Hazards Earth Syst. Sci.* 9, 779–788.
- Bolaños, R., Sanchez-Arcilla, A., Cateura, J., 2007. Evaluation of two atmospheric models for wind–wave modelling in the NW Mediterranean. *J. Mar. Syst.* 65, 336–353.
- Booij, N., Ris, R.C., Holthuijsen, L.H., 1999. A third-generation wave model for coastal regions 1. Model description and validation. *J. Geophys. Res.* 104, 7649–7666.
- Cavaleri, L., Bertotti, L., 2003. The characteristics of wind and wave fields modelled with different resolutions. *Q. J. R. Meteorol. Soc.* 129, 1647–1662.
- Cavaleri, L., Bertotti, L., 1997. In search of the correct wind and wave fields in a minor basin. *Mon. Weather Rev.*, 1964–1975.
- Donelan, M.A., Hamilton, J., Hui, W.H., 1985. Directional spectra of wind-generated waves. *Philos. Trans. R. Soc. Lond. Ser. A: Math. Phys. Sci.* 315, 509–562.
- Grell, G.A., Dudhia, J., and Stauffer, D.R., 1994. Description of the fifth-generation Penn State/NCAR Mesoscale Model (MM5). NCAR Technical Note, NCAR/TN-398-STR.
- Hasselmann, K., Barnett, T.P., Bouws, E., Carlson, D.E., Cartwright, D.E., Enke, K., Ewing, J.A., Gienapp, H., Hasselmann, D.E., Kruseman, P., Meerburg, A., Müller, P., Olbers, D.J., Richter, K., Sell, W., Walden, H., 1973. Measurements of wind-wave growth and swell decay during the Joint North Sea Wave Project (JONSWAP). *Dtsch. Hydrogr. Z.* 8, 1–95.
- Janssen, P.A. E.M., 1991. Quasi-linear theory of wind-wave generation applied to wave forecasting. *J. Phys. Oceanogr.* 21, 1631–1642.
- Kahma, K.K., Calkoen, C.J., 1992. Reconciling discrepancies in the observed growth of wind-generated waves. *J. Phys. Oceanogr.* 1389–1405.
- Komen, G.J., Hasselmann, K., Hasselmann, K., 1984. On the existence of a fully developed wind-sea spectrum. *J. Phys. Oceanogr.* 14, 1271–1285.
- Monbaliu, J., Padilla-Hernandez, R., Hargreaves, J.C., Albiach, J.C.C., Luo, W., Sclavo, M., Günther, H., 2000. The spectral wave model, WAM, adapted for applications with high spatial resolution. *Coast. Eng.* 41, 41–62.
- Niclasen, B.A., 2006. An Operational Wave Model for the Faroe shelf (Ph.D. thesis). University of the Faroe Islands.
- Ponce de León, S., Ocampo-Torres, F.J., 1998. Sensitivity of a wave model to wind variability. *J. Geophys. Res.* 103, 3179–3201.
- Rogers, W.E., Hwang, P.A., Wang, D.W., 2003. Investigation of wave growth and decay in the SWAN model: three regional-scale applications. *J. Phys. Oceanogr.* 366–389.
- Sánchez-Arcilla, A., González-Marco, D., Bolaños, R., 2008. A review of wave climate and prediction along the Spanish Mediterranean coast. *Nat. Hazards Earth Syst. Sci.* 8, 1217–1228.
- The SWAN Team, 2009. SWAN scientific and technical documentation. SWAN Cycle III version 40.72ABCD.
- The WISE Group Cavaleri, L., Alves, J.-G.M., Ardhuin, F., Babanin, A., Banner, M., Belibassakis, K., Benoit, M., Donelan, M., Groeneweg, J., Herbers, T.H.C., Hwang, P., Janssen, P.A. E.M., Janssen, T., Lavrenov, I.V., Magne, R., Monbaliu, J., Onorato, M., Polnikov, V., Resio, D., Rogers, W.E., Sheremet, A., McKee Smith, J., Tolman, H.L., van Vledder, G., Wolf, J., Young, I., 2007. Wave modelling – the state of the art. *Prog. Oceanogr.* 75, 603–674.
- Tolman, H., 2002. Limiters in third-generation wind wave models. *J. Atmos. Ocean. Sci.* 8, 67–83.
- Van der Westhuysen, A.J., Zijlema, M., Battjes, J.A., 2007. Nonlinear saturation-based whitecapping dissipation in SWAN for deep and shallow water. *Coast. Eng.* 54, 151–170.